CRYSTAL GROWTH & DESIGN

Article

pubs.acs.org/crystal

Porous Cadmium(II) Anionic Metal–Organic Frameworks Based on Aromatic Tricarboxylate Ligands: Encapsulation of Protonated Flexible Bis(2-methylimidazolyl) Ligands and Proton Conductivity

Xiaoju Li,*[,†,‡] Xiaofei Sun,[†,‡] Xinxiong Li,[‡] Zhihua Fu,*[,‡] Yanqing Su,[†,‡] and Gang Xu*[,‡]

[†]College of Chemistry and Chemical Engineering, Fujian Normal University, Fuzhou, Fujian 350007, China

[‡]State Key Laboratory of Structural Chemistry, Fujian Institute of Research on the Structure of Matter, Chinese Academy of Sciences, Fuzhou, Fujian 350002, China

Supporting Information

ABSTRACT: Two porous 3-D anionic metal–organic frameworks (MOFs) containing protonated bmib, $[Cd_2(btc)_2(H_2O)_2]_n \cdot n(H_2bmib) \cdot 6n(H_2O)$ (**1**) and $[Cd_4(cpip)_2(Hcpip)_2]_n \cdot n(H_2bmib) \cdot n(H_2O)$ (**2**), have been prepared by hydrothermal reactions of $Cd(NO_3)_2 \cdot 4H_2O$, 1,4-bis(2-methylimidazol-1′-yl)butane (bmib) with 1,3,5-benzenetricarboxylic acid (H_3btc) and 5-(4-carboxyphenoxy)isophthalic acid (H_3cpip), respectively. Complexes **1** and **2** are 3-D anionic frameworks containing 1-D channels and consisting of tetranuclear Cd(II)-carboxylate units, respectively. H_2bmib and lattice water molecules are located in their void spaces and form extensive hydrogen bonds and C–H···π interaction with the anionic frameworks. TGA studies and XRD patterns show the anionic frameworks of **1** and **2** are intact after the removal of lattice water molecules. The luminescent emission of **1** and **2** shows an obvious red shift in comparison with free H_3btc and H_3cpip, respectively. Complexes **1** and **2** possess proton conduction owing to the presence of the extensive hydrogen bonds and protonation of bmib; their proton conductivity at 333 K and 95% relative humidity are 5.4×10^{-5} and 2.2×10^{-5} S cm^{-1}, respectively.

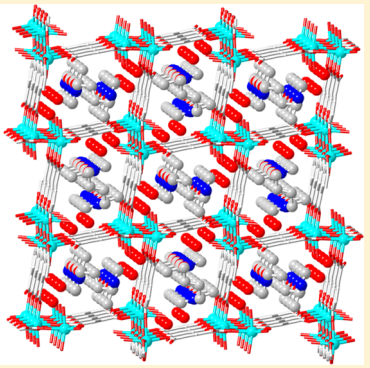

INTRODUCTION

Porous metal–organic frameworks (MOFs) have attracted considerable interests due to their fascinating structures and potential applications in gas adsorption, separation, drug delivery, sensing, and heterogeneous catalysis.[1−7] The use of polynuclear metal clusters as secondary building units (SBUs) has been shown to be a powerful and effective strategy for the construction of porous MOFs. In this context, aromatic di- or polycarboxylate ligands have been popular building blocks to assemble SBUs bearing different sizes and connectivity.[5−9] A large family of porous MOFs has been constructed by deliberate selection of rigid carboxylate ligands and suitable SBUs, their structures and performances can be flexibly modified through adjusting the properties of linkers between carboxylate groups.[8] The introduction of bridging nitrogen-donor ligands into the carboxylate systems can extend metal–carboxylate frameworks through coordinating to SBUs, resulting in the formation of desirable high-dimensional MOFs.[9−14] In addition, they may serve as the essential supports of the porosities in host MOFs with the help of hydrogen bonds and/or $\pi \cdots \pi$ stacking interactions, which exerts a template effect on the topology and dimension of MOFs.

In the construction of porous MOFs, 1,3,5-benzenetricarboxylate (btc) is one of the most widely used ligands owing to its high symmetry, various coordination modes, and strong coordination ability toward metal ions.[15−22] Many porous MOFs based on Cu(II) and Zn(II) ions have been constructed by combining btc with 4-connected $Cu_2(COO)_4$ paddle-wheel SBUs and octahedral 6-connected $Zn_4O(COO)_6$ SBUs.[17−22] Moreover, a large family of isoreticular MOFs have been derived by using these SBUs and this type of tricarboxylate ligands bearing different lengths, pore sizes, shapes, and functionalities.[23−26] Many porous Cd(II) MOFs based on btc and its tricarboxylate analogues have been prepared,[26] but it is difficult to exactly predict or synthesize MOFs consisting of Cd(II)–carboxylate clusters because Cd(II) possesses flexible coordination number from 4 to 7, and it also lacks a strong preference for specific Cd(II)–carboxylate SBUs with well-defined connectivity and point symmetry. The use of mixed ligands of aromatic carboxylates and nitrogen-containing ligands further adds the difficulty to predict structures of target MOFs. It is known that nitrogen-donor ligands not only may be involved in coordination with Cd(II) but also can easily deprotonate carboxylic ligands and concomitantly be protonated in the assembly process owing to strong electron-donating ability, inducing the formation of porous anionic MOFs with protonated nitrogen-donor ligands as templates or guest molecules.[27−30] In our continuous effort to construct

Received: June 9, 2015
Revised: August 3, 2015
Published: August 10, 2015

DOI: 10.1021/acs.cgd.5b00799
Cryst. Growth Des. 2015, 15, 4543−4548

cluster-based MOFs using 5-substituted isophthalates and flexible bis(imidazolyl) ligands,[31,32] herein, we report two porous anionic Cd(II) MOFs containing protonated 1,4-bis(2-methylimidazol-1′-yl)butane (bmib) as guest molecules, $[Cd_2(btc)_2(H_2O)_2]_n \cdot n(H_2bmib) \cdot 6n(H_2O)$ (**1**) and $[Cd_4(cpip)_2(Hcpip)_2]_n \cdot n(H_2bmib) \cdot n(H_2O)$ (**2**). (H_3cpip = 5-(4-carboxyphenoxy)isophthalic acid). Interestingly, these two complexes show proton conductivity owing to the presence of protonated H_2bmib and extensive hydrogen bonds.

EXPERIMENTAL SECTION

Materials and General Methods. H_3cpip[33] and bmib[34] were synthesized according to literature methods; other chemicals were commercially available and used as purchased. IR spectra (KBr pellets) were measured on a Magna 750 FT-IR spectrophotometer in the range of 400−4000 cm^{-1}. Luminescent spectra were measured on an Edinburgh Instruments FLS920 spectrofluorimeter equipped with both continuous-wave (450 W) and pulse xenon lamps. Powder X-ray diffraction data (XRD) were measured on a Philips X'Pert-MPD diffractometer with Cu Kα radiation (λ = 1.54056 Å). Nitrogen adsorption and desorption isotherms were measured at 77 K using a Micromeritics ASAP 2020 system. The samples were degassed at 100 °C for 10 h before the measurements. Surface areas were calculated from the adsorption data using Brunauer−Emmett−Teller (BET). Thermogravimetric analyses (TGA) were performed on a NETSCHZ STA 449C thermoanalyzer under N_2 at a heating rate of 10 °C/min. C, H, and N elemental analyses were performed on an EA1110 CHNS-0 CE element analyzer.

Proton Conductivity Measurement. Proton conductivity measurements were performed in a quasi-four-electrode alternating current (AC) impedance technique using a Solartron 1260 impedance/gain-phase analyzer. The powdered crystalline samples were compressed to 0.6 mm in thickness and 2.5 mm in diameter under a presser of 101 MPa. Two sides of the pellet were connected to gold wires by gold paste. The sample pellet was measured at frequency ranging from 10^7 to 1 Hz by varying temperature from 30 to 60 °C and/or relative humidity (RH) from 40 to 95% RH. The conductivity of the sample was deduced from the Debye semicircle in Nyquist plot.

*Synthesis of $[Cd_2(btc)_2(H_2O)_2]_n \cdot n(H_2bmib) \cdot 6n(H_2O)$ (**1**).* A mixture of H_3btc (22 mg, 0.10 mmol), bmib (22 mg, 0.10 mmol), $Cd(NO_3)_2 \cdot 4H_2O$ (185 mg, 0.60 mmol), and NaOH (0.25 mL, 1 mol·L^{-1}) in deionized water (10 mL) was placed in a Teflon-lined stainless steel vessel (30 mL) and was heated to 160 °C for 3 days. After natural cooling to ambient temperature, colorless crystals of **1** were obtained. Yield: 21 mg [42% based on H_3btc]. Anal. Calcd For $C_{15}H_{20}CdN_2O_{10}$ (500.73): C, 35.97; H, 4.03; N, 5.59. Found: C, 36.33; H, 4.18; N, 5.58. IR (KBr, cm^{-1}): 3468(vw), 3065(vw), 2664(vw), 1926(vw), 1640(vw), 1606(s), 1545(s), 1445(m), 1388(vs), 1274(m), 1166(w), 917(vw), 724(vs), 697(m), 543(w).

*Synthesis of $[Cd_4(cpip)_2(Hcpip)_2]_n \cdot n(H_2bmib) \cdot n(H_2O)$ (**2**).* A mixture of H_3cpip (30 mg, 0.10 mmol), bmib (22 mg, 0.10 mmol), $Cd(NO_3)_2 \cdot 4H_2O$ (90 mg, 0.30 mmol), and NaOH (0.25 mL, 1 mol·L^{-1}) in deionized water (15 mL) was placed in a Teflon-lined stainless steel vessel (30 mL) and was heated to 130 °C for 2 days. After natural cooling to ambient temperature, colorless crystals of **2** were obtained. Yield: 42 mg [40% based on H_3cpip]. Anal. Calcd For $C_{36}H_{26}Cd_2N_2O_{14.50}$ (943.39): C, 45.83; H, 2.77; N, 2.96. Found: C, 45.78; H, 2.77; N, 2.97. IR (KBr, cm^{-1}): 3408(vw), 1674(vw), 1597(vw), 1551(s), 1453(w), 1371(m), 1307(w), 1257(m), 1222(w), 1167(vw), 975(w), 782(vw), 733(w).

X-ray Crystallography. Single crystals of complexes **1** and **2** were mounted on a glass fiber for X-ray diffraction analysis. Data sets were collected on a Rigaku AFC7R equipped with a graphite-monochromated Mo−Kα radiation (λ = 0.71073 Å) from a rotating anode generator at 293 K. Intensities were corrected for LP factors and empirical absorption using the ψ scan technique. The structures were solved by direct methods and refined on F^2 with full-matrix least-squares techniques using the SHELX-97 program package.[35,36] All non-hydrogen atoms were refined anisotropically. The hydrogen atoms of water molecules and protons in the protonated bmib were located from the difference Fourier map and refined isotropically. The positions of other hydrogen atoms were generated geometrically (C−H bond fixed at 0.96 Å), assigned isotropic thermal parameters, and allowed to ride on their parent carbon atoms before the final cycle of refinement. Crystal data and the details of data collection for complexes **1** and **2** are summarized in Table S1. The selected bond distances and bond angles are given in Table S2. Crystallographic data of **1** and **2** have been deposited in the Cambridge Crystallographic Data Centre as supplementary publication with CCDC number: 1037216 and 1037217.

RESULTS AND DISCUSSION

Synthesis. It is known that reaction conditions, such as solvent, temperature, ratio of metal to ligand, and pH value, have important effects on the assembly of aromatic carboxylates and nitrogen-containing ligands with metal ions. A series of experiments were attempted in order to produce single crystals with good quality and purity. Complex **1** is readily available by hydrothermal reaction of H_3btc, bmib, and $Cd(NO_3)_2 \cdot 4H_2O$ in the presence of NaOH at 160 °C, the replacement of H_3btc by H_3cpip at 130 °C gave rise to complex **2** in a good yield. It should be mentioned that natural cooling from reaction temperature to ambient temperature is important for the formation of pure **1** and **2**. When reaction temperature was lowered to ambient temperature at a rate of 3 or 5 °C·h^{-1}, **1** and **2** were accompanied by the impurities. Base is also necessary for the formation of **1** and **2**, the absence of NaOH provides uncharacterized floccules under the same conditions. The synthesis of **2** was also attempted at 160 °C; the desirable product was obtained in low yield with the concomitant formation of uncharacterized powders.

Structural Descriptions. *Crystal Structure of $[Cd_2(btc)_2(H_2O)_2]_n \cdot n(H_2bmib) \cdot 6n(H_2O)$ (**1**).* Complex **1** crystallizes in the monoclinic space group $P2_1/c$ and is an ionic 3-D porous structure containing 1-D channels. The asymmetry unit is composed of one btc, one Cd(II), one coordinated water molecule, half of bmib, and three free water molecules. To achieve overall charge balance, water molecules, btc, or bmib are required to be protonated. 2-Methylimidazolyl nitrogen atoms of bmib are known to possess stronger electron-donating ability than water molecules, and the bond angles and distances in three carboxylate groups of btc are in the normal range. As a result, the protonation likely occurs at nitrogen atoms of bmib. The coordination environments of Cd(II) ions are shown in Figure 1a, two Cd(II) ions are equivalently bridged by two μ_2,η^2-carboxylate groups from different btc to form a dinuclear Cd(II)-carboxylate SBU. The SBU has a crystallographic inversion center at the middle of Cd1−Cd1D core, and the Cd1···Cd1A distance is 3.957 Å. Cd(II) adopts a highly distorted octahedral geometry, and it is coordinated by one monodentate carboxylate atom and one water molecule at the axial positions with O1W−Cd1−O5C bond angle being 148.2(2)°. The equatorial plane is composed of two oxygen atoms of one chelating carboxylate group (O3B and O4B) and two oxygen atoms (O1 and O2A) of different μ_2,η^2-carboxylate. The Cd(II) ion is approximately coplanar with four equatorial atoms with a mean deviation of 0.1832 Å. btc serves as a μ_4-bridge through its μ_2,η^2-bridging, chelating and monodentate carboxylate groups coordinating to four Cd(II) ions (Scheme 1a). Interestingly, μ_2,η^2-bridging and chelating carboxylate in btc link dinuclear Cd(II) SBUs into a 1-D chain (Figure S1). The closest Cd···Cd separation across btc in the chain is 7.781

DOI: 10.1021/acs.cgd.5b00799
Cryst. Growth Des. 2015, 15, 4543−4548

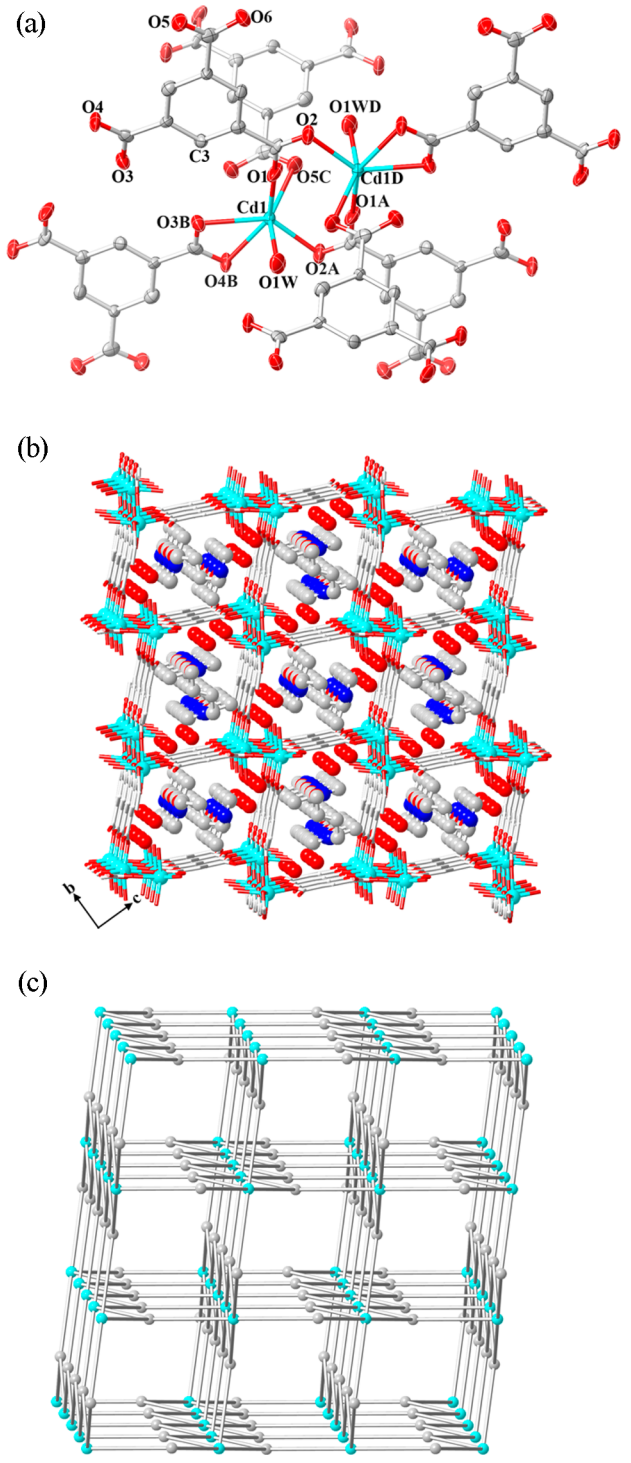

Figure 1. (a) View of the coordination environment of dinuclear Cd(II) SBU in complex **1** with thermal ellipsoid at 50% level. (b) View of 3-D porous structure along the *a* axis in complex **1**. (c) View of the (3,6)-connected topology in the anionic framework of complex **1**.

Å. Further linkage of such chains by monodentate carboxylate group gives rise to a 3-D anionic framework containing 1-D channels (Figure 1b). The accessible void volume is 56.9% per unit cell volume as calculated by PLATON. The protonated bmib and free water molecules are located in the large void space. Notably, 2-methylimidazolyl ring of bmib and phenyl ring of btc form $\pi\cdots\pi$ stacking interaction with center-to-center distance being 3.725 Å. The extensive hydrogen bonds between coordination water and carboxylate oxygen atoms [O1W–H···O5^{i} 2.771(10) Å, O2W–H···O4^{ii} 2.745(10) Å, O3W–H···O6^{iii} 2.837(10) Å, O3W–H···O3^{iv} 2.807(9) Å, O4W–H···O2^{v} 2.879 Å; symmetry code: (i) $x - 1/2, -y - 1/2, z + 1/2$; (ii) $x - 1/2, -y - 1/2, z + 1/2$; (iii) $x + 1/2, -y - 1/2, z + 1/2$; (iv) $-x + 1, -y, -z + 1$; (v) $1/2 + x, -y - 1/2, 1/2 + z$], between protonated 2-methylimidazolyl nitrogen atom and water molecule [N2–H···O4W 2.771(13) Å] as well as between water molecules [O1W–H···O2W 2.787(11) Å, O2W–H···O3W 2.751(11) Å, O4W–H···O2W^{vi} 2.877(12) Å; symmetry code: (vi) $x + 1/2, -y - 1/2, z - 1/2$] further consolidate the structural framework. Topological analysis was performed to better understand the anionic framework. If taking dinuclear Cd(II) SBU as one node, each SBU becomes a four-connected node owing to two adjacent SBUs bridged by two btc; btc can be regarded as a three-connected vertex. The interconnection of three identical SBUs and four btc generates a 3,6-connected topology with the Schläfli symbol being $\{4\cdot6^2\}_2\{4^2\cdot6^{10}\cdot8^3\}$ (Figure 1c).

Crystal Structure of $[Cd_4(cpip)_2(Hcpip)_2]_n\cdot n(H_2bmib)\cdot n(H_2O)$ (**2**). Complex **2** also crystallizes in the monoclinic space group $P2_1/c$ and possesses a 3-D anionic framework consisting of tetranuclear Cd(II)-carboxylate units. The asymmetric unit contains two crystallographically independent Cd(II) ions, one completely deprotonated cpip, one partially deprotonated Hcpip, half of protonated bmib, and half of free water molecule. The C30–O13 bond distance in one carboxyl group of Hcpip is 1.318(5) Å, which is much longer than other analogues in the range from 1.220(4) to 1.275(4) Å; moreover, the carboxylic proton is readily located crystallographically and resides on one oxygen atom of carboxyl group in Hcpip. As a result, H_3cpip is partially deprotonated, and one carboxyl group in Hcpip can be assigned as carboxylic group. To further balance the negative charge, it is acceptable that bmib is protonated owing to strong electron-donating ability of 2-methylimidazolyl nitrogen atoms than water molecules, and the corresponding protons are also defined crystallographically on 2-methylimidazolyl nitrogen atoms. The coordination environments of Cd(II) ions are shown in Figure 2a, Cd(1) is hepta-coordinated, while Cd(2) is in a distorted octahedral geometry. Cd(1) and Cd(2) are bridged by two μ_2-chelating/bridging carboxylate groups (O4B, O5B, O6, and O7) and one μ_2,η^2-carboxylate group (O1C and O2C) from three different cpip to form a dinuclear Cd(II)-carboxylate subunit. The Cd(1)···Cd(2) distance in the subunit is 3.546 Å, which is much shorter than that in complex **1**. Besides oxygen atoms from bridging carboxylate groups (O2C, O4B, O6, and O7), two oxygen atoms of one chelating carboxylate group (O8 and O9), and one carboxylic oxygen atom (O14D) from different Hcpip complete hepta-coordinated environment of Cd(1) ion. The equatorial plane of Cd2 is defined by two oxygen atoms from μ_2-chelating/bridging carboxylate group (O4B and O5B) in cpip, one μ_2,η^2-carboxylate oxygen atom from cpip (O1C), and one μ_2,η^2-carboxylate oxygen atom (O10E) from Hcpip. The deviation of Cd2 from the equatorial plane is 0.2254 Å. One μ-oxygen atom of μ_2-chelating/bridging carboxylate from cpip (O6) and one μ_2,η^2-carboxylate oxygen atom from Hcpip (O11A) occupy the axial positions with O11A–Cd2–O6 bond angle being 169.56(9)°. Interestingly, two μ_2,η^2-carboxylate groups from different Hcpip connect Cd2 and symmetry-related Cd2F to form a tetranuclear Cd(II)-carboxylate SBU (Figure S2), the Cd2···Cd2F distance in the SBU is 3.933 Å, which is similar to that in complex **1**. cpip serves as a μ_6-bridge

DOI: 10.1021/acs.cgd.5b00799
Cryst. Growth Des. 2015, 15, 4543–4548

Scheme 1. Coordination Mode of btc, cpip, and Hcpip

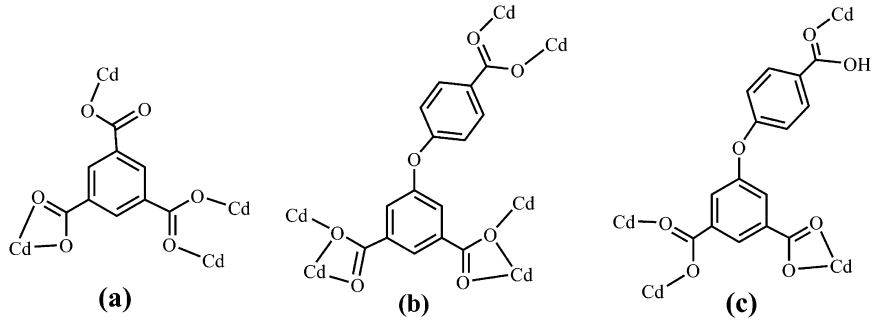

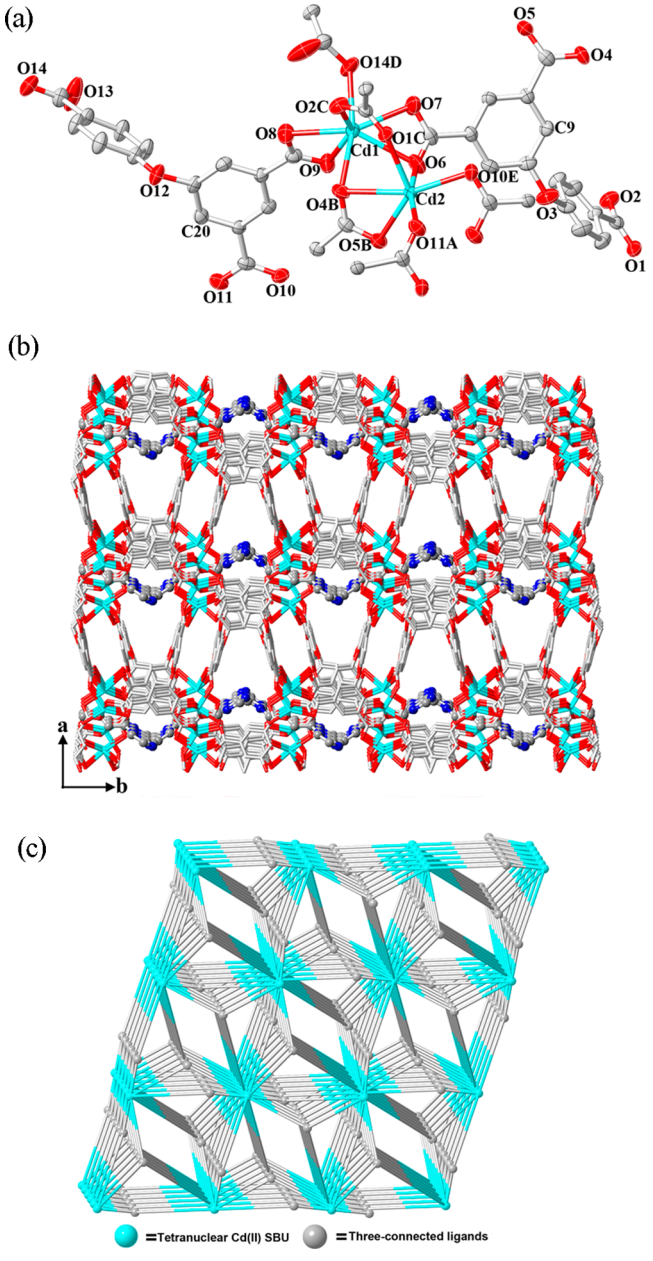

Figure 2. (a) View of the coordination environment of Cd1 and Cd2 in complex **2** with thermal ellipsoid at 50% level. (b) View of 3-D porous structure with H_2bmib guest molecules along the *c* axis in complex **2**. (c) View of the (3,3,12)-connected topology in anionic framework of complex **2**.

using its two μ_2-chelating/bridging carboxylate groups and one μ_2,η^2-carboxylate group (Scheme 1b). Two phenyl rings in cpip are almost perpendicular to each other with the dihedral angle between them of 79.588(11)°. cpip links dinuclear Cd(1) and Cd(2) subunits into a 2-D layer (Figure S3). Further connection by Hcpip generates a 3-D anionic network consisting of tetranuclear Cd(II) units (Figure 2b) in which Hcpip acts as a μ_4-bridge through its one μ_2,η^2-carboxylate group, one chelating carboxylate group, and one monodentate carboxylic group (Scheme 1c). The twisting angle between two phenyl rings in Hcpip is 72.285(15)°, which is smaller than that from cpip. PLATON analysis shows that the accessible void volume is 27.4% per unit cell volume. The large voids are filled by water molecules and H_2bmib. Notably, the phenyl ring of Hcpip and the protonated 2-methylimidazolyl ring form C–H···π interaction with the distance of carbon to the center of imidazolyl ring being 3.150 Å. The extensive hydrogen bonds between carboxylic and carboxylate [O13–H···O2^{i} 2.719(4) Å; symmetry code: (i) $-x+1, y-1/2, -z-1/2$], between protonated 2-methylimidazolyl and carboxylate [N1–H···O1^{ii} 2.823(4) Å; symmetry code: (ii) $-x+2, y-1/2, -z+1/2$], and between water and carboxylate [O1W–H···O11 2.904 Å] further consolidate the whole framework. To have a better insight into the fascinating 3-D structure, topological analysis is given. Taking the tetranuclear Cd(II) SBU as one node, each SBU becomes a 12-connected node; cpip and Hcpip can be regarded as two independent three-connected vertices. The interlinkage of these tetranuclear SBUs with three-connected cpip and Hcpip results in the formation of an unprecedented 3,3,12-connected topology (Figure 2c). The Schläfli symbol of this net is $\{4^2\cdot6\}_4\{4^8\cdot6^{45}\cdot8^{13}\}$.

Thermal Properties. In order to characterize thermal stability of **1** and **2**, thermogravimetric analyses (TGA) of as-synthesized samples were performed under nitrogen atmosphere (Figure S4). In **1**, the weight loss of 14.01% before 130 °C is attributed to the removal of lattice and coordinated water molecules (calcd: 14.37%); the host framework of **1** is stable up to 320 °C. In **2**, the weight loss of free water molecules occurs before 120 °C (obsd: 0.91%, calcd: 0.95%), and the framework starts to collapse after 390 °C.

Powder XRD and Gas Sorption Studies. In order to check the purity and homogeneity, as-synthesized samples of **1** and **2** were measured by powder XRD at room temperature. As shown in Figures 4 and 5, the peak positions of experimental patterns are in good agreement with the simulated ones, which clearly indicates good purity of **1** and **2**. When as-synthesized samples of complex **1** were heated to 140 °C, XRD patterns show that the anionic framework of complex **1** is still intact, while it begins to collapses upon treatment at 300 °C (Figure

DOI: 10.1021/acs.cgd.5b00799
Cryst. Growth Des. 2015, 15, 4543–4548

3). However, the anionic framework of complex **2** is stable upon the treatment at 230 and 340 °C as confirmed by XRD patterns (Figure 4).

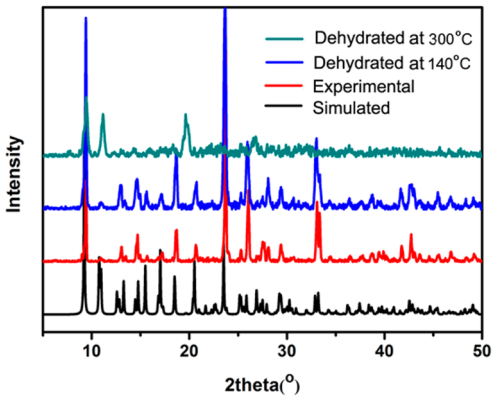

Figure 3. XRD patterns for complex **1**.

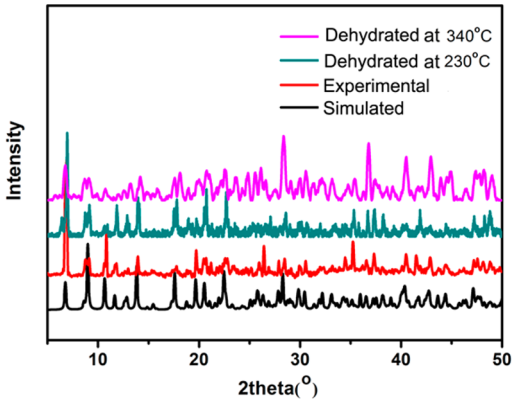

Figure 4. XRD pattern for complex **2**.

The N_2 sorption at 77 K of **1** and **2** was conducted after as-synthesized samples were heated at 140 °C for 10 h. However, their gas uptake is almost negligible, which is probably ascribed to the pore blocking by the protonated H_2bmib.

Proton Conductivity. Proton conductivities of **1** and **2** were evaluated by AC impedance/gain-phase analyzer using a compacted pellet of the powdered crystalline samples. Both **1** and **2** show RH-dependent conductivity. As shown in Figure 5a, the conductivity of **1** gradually increases 4 orders of magnitude and reaches to 6.7×10^{-6} S cm^{-1} by varying RH from 40 to 95% at room temperature. The conductivity of **2** has similar variation behavior with respect to RH, and its highest conductivity is 9.2×10^{-6} S cm^{-1} (Figure 5c). However, **2** has very low conductivity before 80% RH, which cannot be detected by our equipment. The conductivities of **1** and **2** have medium value at high humidity and are comparable to the reported MOF materials.[37−46] Figure 5b,d shows temperature-dependent conductivity for these two complexes at 95% RH; **1** and **2** possess the highest conductivity of 5.4×10^{-5} and 2.2×10^{-5} S cm^{-1} at 60 °C, respectively. The proton conductivity in **1** and **2** are probably ascribed to the presence of the extensive hydrogen bonds and protonation of bmib. From the least-squares fits of the slopes, the activation energy of proton conductivity of **1** and **2** are calculated to be 0.62 and 0.27 eV, respectively. The difference of the activation energy is probably

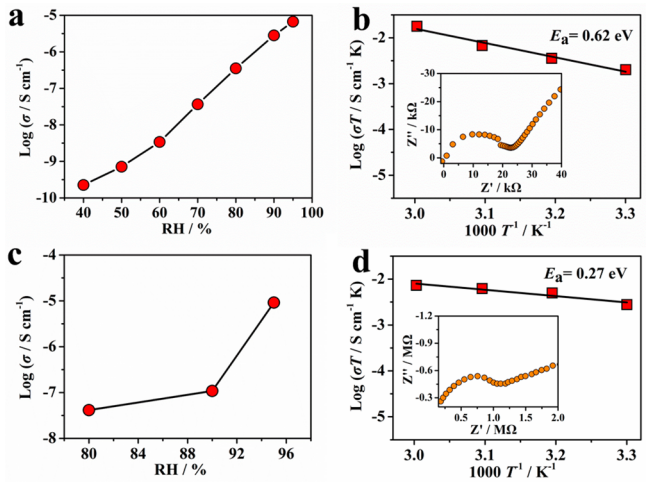

Figure 5. Proton conductivity of **1** (a) and **2** (c) under various RH conditions at room temperature. Arrhenius plots of the proton conductivity of **1** (b) and **2** (d) under 95% RH; least-squares fitting is shown as a solid line. Inset: typical Nyquist plots of **1** and **2** measured at room temperature.

ascribed to their different supramolecular interactions. The conductive protons in complex **1** result from the protonated bmib, while they are from the protonated bmib and carboxylic acid of Hcpip in **2**. The proton densities in the unit cell of **1** and **2** are 2.13×10^{-3} and 2.28×10^{-3} Å^3, respectively, which are very close to each other. It is known that the stronger supramolecular interactions (hydrogen bonding, $\pi\cdots\pi$ stacking interaction, and van der Waals) of the protonated molecules with surrounding molecules are, the more difficult it is for them to motion freely, which results in higher activation energy for proton transport.[47] Based on crystal structure analysis, H_2bmib in **1** possesses a strong hydrogen bonding interaction with lattice water molecule [N−H···OW 2.771(13) Å] and a $\pi\cdots\pi$ stacking interaction with the phenyl ring of btc, while H_2bmib in **2** shows a hydrogen bonding interaction with carboxylate oxygen of Hcpip [N−H···O1 2.823(4) Å] and a C−H···π interaction with the phenyl ring of Hcpip. Obviously, the supramolecular interactions in **2** are much weaker than that in **1**. In addition, there are four carboxylic groups in one unit cell of **2**, which possesses smaller size than the protonated 2-methylimidazolyl and may motion more freely. Based on the activation energy of proton conductivity, the mechanism of proton conductivity of **1** may be assigned as vehicle mechanism owing to its activation energy above 0.5 eV,[48] while complex **2** follows Grotthuss mechanism owing to its activation energy among 0.1−0.4 eV.[49]

CONCLUSIONS

Two porous 3-D Cd(II) MOFs have been constructed using aromatic tricarboxylate ligands and flexible bis(2-methylimidazolyl) ligand (bmib). The dinuclear and tetranuclear Cd(II)-carboxylate SBUs were formed, respectively. btc in complex **1** connects dinuclear SBUs into a 3-D anionic framework containing 1-D channels, while cpip and Hcpip complex **2** link tetranuclear SBUs into a porous 3-D anionic framework. bmib is not involved in coordination, it is protonated to balance charge and to serve as guest molecules. The void cavums of the anionic frameworks in these two MOFs are filled by H_2bmib and lattice water molecules. H_2bmib forms hydrogen bonds, $\pi\cdots\pi$ stacking, and C−H···π interaction with the anionic

DOI: 10.1021/acs.cgd.5b00799
Cryst. Growth Des. 2015, 15, 4543−4548

frameworks, which are helpful for stabilization of the ionic frameworks. The extensive hydrogen bonds and the presence of protonated H_2bmib are responsible for proton conductivity of these two complexes. In summary, this study provides an attractive approach for the construction of anionic frameworks, which is helpful for development of ionic MOFs.

■ ASSOCIATED CONTENT

Supporting Information

The Supporting Information is available free of charge on the ACS Publications website at DOI: 10.1021/acs.cgd.5b00799.

Additional figures, TGA curves, selected bond lengths and angles, photoluminescent spectra, and corresponding descriptions of properties (PDF)
X-ray crystallographic file for **1** (CIF)
X-ray crystallographic file for **2** (CIF)

■ AUTHOR INFORMATION

Corresponding Authors

*E-mail: xiaojuli@fjnu.edu.cn.
*E-mail: zhihuafu@fjirsm.ac.cn.
*E-mail: gxu@fjirsm.ac.cn.

Notes

The authors declare no competing financial interest.

■ ACKNOWLEDGMENTS

This work was supported by the National Natural Science Foundation of China (51402293, 21401193), the Natural Science Foundation of Fujian (2015J01038), and State Key Laboratory of Structural Chemistry (20150015).

■ REFERENCES

(1) Férey, G. *Chem. Soc. Rev.* **2008**, *37*, 191−214.
(2) Mukherjee, S.; Mukherjee, P. S. *Acc. Chem. Res.* **2013**, *46*, 2556−2566.
(3) Lu, W. G.; Wei, Z. W.; Gu, Z. Y.; Liu, T. F.; Park, J.; Tian, J.; Zhang, M. W.; Zhang, Q.; Bosch, M.; Zhou, H. C. *Chem. Soc. Rev.* **2014**, *43*, 5561−5593.
(4) Li, X. X.; Xu, H. Y.; Kong, F. Z.; Wang, R. H. *Angew. Chem., Int. Ed.* **2013**, *52*, 13769−13773.
(5) Genna, D. T.; Wong-Foy, A. G.; Matzger, A. J.; Sanford, M. S. *J. Am. Chem. Soc.* **2013**, *135*, 10586−10589.
(6) Jeong, S.; Kim, D.; Shin, S.; Moon, D.; Cho, S. J.; Lah, M. S. *Chem. Mater.* **2014**, *26*, 1711−1719.
(7) Morris, R. E.; Wheatley, P. S. *Angew. Chem., Int. Ed.* **2008**, *47*, 4966−4981.
(8) Tranchemontagne, D. J.; Mendoza-Cortes, J. L.; O'Keeffe, M.; Yaghi, O. M. *Chem. Soc. Rev.* **2009**, *38*, 1257−1283.
(9) Hu, F. L.; Wu, W.; Liang, P.; Gu, Y. Q.; Zhu, L. G.; Wei, H.; Lang, J. P. *Cryst. Growth Des.* **2013**, *13*, 5050−5061.
(10) Cheng, H. J.; Li, H. X.; Ren, Z. G.; Lü, C. N.; Shi, J.; Lang, J. P. *CrystEngComm* **2012**, *14*, 6064−6071.
(11) Zhao, W.; Fan, J.; Song, Y.; Kawaguchi, H.; Okamura, T.; Sun, W. Y.; Ueyama, N. *Dalton Trans.* **2005**, 1509−1517.
(12) Cheng, H. J.; Wu, B.; Zhu, L. W.; Ni, C. Y.; Dai, M.; Li, H. X.; Ren, Z. G.; Lang, J. P. *Inorg. Chem. Commun.* **2013**, *31*, 13−17.
(13) Qin, L.; Hu, J. S.; Li, Y. Z.; Zheng, H. G. *Cryst. Growth Des.* **2012**, *12*, 403−413.
(14) Zhou, X. P.; Xu, Z. T.; Zeller, M.; Hunter, A. D.; Che, C. M. *Inorg. Chem.* **2011**, *50*, 7142−7149.
(15) Matsuda, R.; Kitaura, R.; Kitagawa, S.; Kubota, Y.; Kobayashi, T. C.; Horike, S.; Takata, M. *J. Am. Chem. Soc.* **2004**, *126*, 14063−14070.
(16) Wang, Z. Q.; Kravtsov, V. C.; Zaworotko, M. J. *Angew. Chem., Int. Ed.* **2005**, *44*, 2877−2880.
(17) Zhao, X.; Xiao, B.; Fletcher, A.; Thomas, K. M.; Bradshaw, D.; Rosseinsky, M. J. *Science* **2004**, *306*, 1012−1015.
(18) Deng, H. X.; Doonan, C. J.; Furukawa, H.; Ferreira, R. B.; Towne, J.; Knobler, C. B.; Wang, B.; Yaghi, O. M. *Science* **2010**, *327*, 846−850.
(19) Davies, K.; Bourne, S. A.; Öhrström, L.; Oliver, C. L. *Dalton Trans.* **2010**, *39*, 2869−2874.
(20) Zhang, P.; Li, B.; Zhao, Y.; Meng, X. G.; Zhang, T. L. *Chem. Commun.* **2011**, *47*, 7722−7724.
(21) He, H. M.; Du, J. S.; Su, H. M.; Yuan, Y. H.; Song, Y.; Sun, F. X. *CrystEngComm* **2015**, *17*, 1201−1209.
(22) Kim, D.; Song, X. K.; Yoon, J. H.; Lah, M. S. *Cryst. Growth Des.* **2012**, *12*, 4186−4193.
(23) Liu, W. Y.; He, H. M.; Song, Y.; Du, J. S.; Sun, F. X. *Inorg. Chem. Commun.* **2015**, *57*, 11−14.
(24) Ordonez, C.; Fonari, M.; Lindline, J.; Wei, Q.; Timofeeva, T. *Cryst. Growth Des.* **2014**, *14*, 5452−5465.
(25) Wen, L. L.; Wang, F.; Feng, J.; Lv, K. L.; Wang, C. G.; Li, D. F. *Cryst. Growth Des.* **2009**, *9*, 3581−3589.
(26) Liu, D. M.; Lu, K. D.; Poon, C.; Lin, W. B. *Inorg. Chem.* **2014**, *53*, 1916−1924.
(27) Liu, F. J.; Hao, H. J.; Sun, C. J.; Lin, X. H.; Chen, H. P.; Huang, R. B.; Zheng, L. S. *Cryst. Growth Des.* **2012**, *12*, 2004−2012.
(28) Wang, X. J.; Liu, Y. H.; Xu, C. Y.; Guo, Q. Q.; Hou, H. W.; Fan, Y. T. *Cryst. Growth Des.* **2012**, *12*, 2435−2444.
(29) Mu, Y. J.; Fu, J. H.; Song, Y. J.; Li, Z.; Hou, H. W.; Fan, Y. T. *Cryst. Growth Des.* **2011**, *11*, 2183−2193.
(30) Collman, J. P.; Brauman, J. I.; Fitzgerald, J. P.; Hampton, P. D.; Naruta, Y.; Sparapany, J. W.; Ibers, J. A. *J. Am. Chem. Soc.* **1988**, *110*, 3477−3486.
(31) Li, X. J.; Yu, Z. J.; Guan, T. N.; Li, X. X.; Ma, G. C.; Guo, X. F. *Cryst. Growth Des.* **2015**, *15*, 278−290.
(32) Li, X. J.; Guan, T. N.; Guo, X. F.; Li, X. X.; Yu, Z. J. *Eur. J. Inorg. Chem.* **2014**, *2014*, 2307−2316.
(33) Lama, P.; Aijaz, A.; Sañudo, E. C.; Bharadwaj, P. K. *Cryst. Growth Des.* **2010**, *10*, 283−290.
(34) Huang, X. Y.; Yue, K. F.; Jin, J. C.; Liu, J. Q.; Wang, C. J.; Wang, Y. Y. *Inorg. Chem. Commun.* **2010**, *13*, 338−341.
(35) Sheldrick, G. M. *SHELXS-97, Program for the Crystal Structure Solution*; University of Göttingen: Göttingen, Germany, 1997.
(36) Sheldrick, G. M. *SHELXL-97, Program for the Refinement of Crystal Structure*; University of Göttingen: Göttingen, Germany, 1997.
(37) Mallick, A.; Kundu, T.; Banerjee, R. *Chem. Commun.* **2012**, *48*, 8829−8831.
(38) Dey, C.; Kundu, T.; Banerjee, R. *Chem. Commun.* **2012**, *48*, 266−268.
(39) Dong, X. Y.; Wang, R.; Li, J. B.; Zang, S. Q.; Hou, H. W.; Mak, T. C. W. *Chem. Commun.* **2013**, *49*, 10590−10592.
(40) Horike, S.; Umeyama, D.; Kitagawa, S. *Acc. Chem. Res.* **2013**, *46*, 2376−2384.
(41) Taylor, J. M.; Dawson, K. W.; Shimizu, G. K. *J. Am. Chem. Soc.* **2013**, *135*, 1193−1196.
(42) Chandra, S.; Kundu, T.; Kandambeth, S.; BabaRao, R.; Marathe, Y.; Kunjir, S. M.; Banerjee, R. *J. Am. Chem. Soc.* **2014**, *136*, 6570−6573.
(43) Liang, X.; Zhang, F.; Zhao, H.; Ye, W.; Long, L.; Zhu, G. *Chem. Commun.* **2014**, *50*, 6513−6516.
(44) Zhao, S. N.; Song, X. Z.; Zhu, M.; Meng, X.; Wu, L. L.; Song, S. Y.; Wang, C.; Zhang, H. J. *Dalton Trans.* **2015**, *44*, 948−954.
(45) Sanda, S.; Biswas, S.; Konar, S. *Inorg. Chem.* **2015**, *54*, 1218−1222.
(46) Ramaswamy, P.; Wong, N. E.; Shimizu, G. K. H. *Chem. Soc. Rev.* **2014**, *43*, 5913−5932.
(47) Taylor, J. M.; Dekura, S.; Ikeda, R.; Kitagawa, H. *Chem. Mater.* **2015**, *27*, 2286−2289.
(48) Shigematsu, A.; Yamada, T.; Kitagawa, H. *J. Am. Chem. Soc.* **2011**, *133*, 2034−2036.
(49) Xu, G.; Otsubo, K.; Yamada, T.; Sakaida, S.; Kitagawa, H. *J. Am. Chem. Soc.* **2013**, *135*, 7438−7441.

DOI: 10.1021/acs.cgd.5b00799
Cryst. Growth Des. 2015, 15, 4543−4548